Gómez-Díaz *et al. Geothermal Energy* (2022) 10:7
https://doi.org/10.1186/s40517-022-00217-3

Geothermal Energy

RESEARCH Open Access

Numerical modeling of reinjection and tracer transport in a shallow aquifer, Nesjavellir Geothermal System, Iceland

Esteban Gómez-Díaz[1,2*], Samuel Scott[2,3], Thomas Ratouis[4] and Juliet Newson[2]

*Correspondence:
e.gomez@geol.rwth-aachen.de
[1] Energy and Minerals Resources Group, Geological Institute, RWTH Aachen University, Wüllnerstraße 2, 52056 Aachen, Germany
Full list of author information is available at the end of the article

Abstract

Reinjection of excess water from the power production process in the Nesjavellir geothermal field has increased the temperature of shallow groundwaters, posing a risk to cold water wells used for the power plant as well as the ecosystem in Lake Thingvellir. Here, we present a numerical model of fluid flow and heat transport in the shallow reinjection zone to elucidate the flow path of reinjected liquid and the impact of reinjection on the temperature of groundwaters. The permeability structure of the model is based on a 3D geological model of the area. The numerical simulation is calibrated against underground water temperature data measured between 1998 and 2018 and data from a tracer test performed in 2018–2019. The model reproduces the overall temperature field and shows how a high-permeability lava flow together with rift-parallel normal faults act as permeable channels controlling fluid transport. If injection continues, the temperature along the lava flow increases considerably and spreads vertically to much deeper levels, generating a narrow warm zone along the main fault. If shallow injection ceases, temperature drops rapidly at the surface, but decreases slowly around the reinjection zone over 20 years. The numerical model in this study allowed a better characterization of the fracture–matrix interface and the porosity of post-glacial lava flows, contributing to sustainable management of the geothermal resource and the surrounding environment.

Keywords: Numerical modeling, Geothermal reinjection, Dual porosity, MINC, Tracer injection, Fluid flow, Heat transfer

Introduction

Power generation from high-enthalpy liquid dominated geothermal systems requires the reinjection of significant quantities of hot water (40–80 °C) remaining after the power generation process. The reinjection of this liquid in nearby wells can ensure the longevity of a geothermal resource by providing pressure support, improve heat recovery from the subsurface rock, and reduce the risk of subsidence, in addition to providing an environmentally friendly means of waste disposal (Stefansson 1997; Axelsson 2008, 2012; Kaya et al. 2011; Kamila et al. 2021). Depending on the depth and location of reinjection wells and overall fluid flow patterns, the negative effects of reinjection include be heating of shallow groundwaters, cooling of nearby production wells, ground subsidence (due to rock cooling

and contraction), quenching of productive steam zones and induced seismicity (Diaz et al. 2016). Therefore, reinjection strategies must be carefully planned and monitored.

Tracer testing is one of the primary ways to assess the impact of fluid reinjection on surrounding groundwaters. The technique uses natural or induced variations in fluid chemistry or properties to obtain information about groundwater flow rates and directions, aquifer hydraulic and transport properties, and fluid–rock interaction (Axelsson 2013; Maliva 2016). In the geothermal context, tracer testing is used to assess the nature and properties of hydraulic connections, or flow paths, between reinjection and production wells and to predict the rate of cooling of the production wells in response to long-term reinjection (Rose et al. 2010; Axelsson 2012, 2013).

Results from tracer tests are commonly interpreted using analytical models that assume idealized one-dimensional flow channels connecting reinjection and production boreholes (Shook 2005; Shook and Forsmann 2005; Axelsson 2013). Such models can simulate tracer return profiles quite accurately and yield estimates of the volumetric and hydraulic properties of the reservoir and flow channel. However, it is more challenging to match measured tracer returns with the three-dimensional numerical reservoir models more commonly used to investigate and optimize production and reinjection strategies for large-scale geothermal system management (O'Sullivan et al. 2016). While such models are commonly calibrated with measured downhole temperature and pressure data as well as production history data (enthalpy, mass flow rate, fluid pressure), tracer tests provide an additional source of data that can be used for model calibration, providing high resolution insight into the geometry and hydraulic properties of flow paths. Previous studies using tracer test data to calibrate three-dimensional geothermal reservoir models have shown that a dual-porosity approach is critical to reproduce the fast return profiles, and that good knowledge of the geometry of subsurface fractures is necessary in order to yield model predictions that resemble the measured data (Pham et al. 2010; Buscarlet et al. 2015; Ratouis et al. 2019, 2022).

In this study, we present a three-dimensional numerical simulation of shallow reinjection in the Nesjavellir geothermal field. The model is constrained by geological data, tracer tests conducted at the site from August 2018 to September 2019 and groundwater temperature data from 1998 until 2019. The aim of the research is to understand and characterize the flow paths of reinjected water and forecast the impact of continued reinjection on thermal pollution of the nearby Lake Thingvellir and associated shallow groundwaters.

Nesjavellir Geothermal Power Station

The Nesjavellir Geothermal Power Station (NGPS) is located within the Hengill area of the Western Volcanic Zone in SW-Iceland, roughly 25 km east of Reykjavik (Fig. 1). The NGPS is the second-largest geothermal power station in the country, generating 120 MWe of electricity and 290 MWth of thermal energy for district heating. The power plant uses a combined cycle, wherein a steam is separated at 200 °C and 14 bars, and passed through four steam turbines, requiring 240 kg/s of steam in total. The steam is condensed in a tubular condenser and cooled to approximately 55 °C with cold groundwater, provided by a shallow fresh-water aquifer (Grámelur) in the lava field 6 km away from the power plant, directly to the south of Lake Thingvellir. The cooling water is

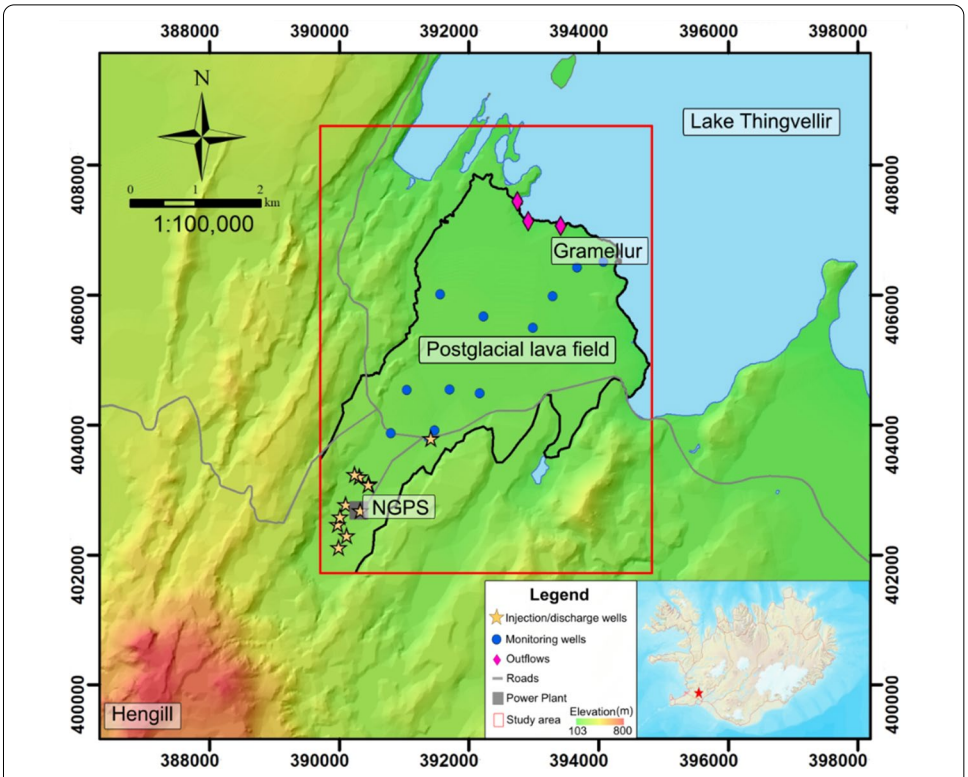

Fig. 1 Location of the Nesjavellir geothermal field. Red box is the study zone, and the main area of interest is within the post-glacial lava field outlined by the black line. NGPS: Nesjavellir Geothermal Power Station

heated in a heat exchanger to 87 °C by the ~ 190 °C hot geothermal water derived from the separators (Gíslason 2000).

Much of the excess water derived from the condensed steam and separated liquid is discharged either into shallow reinjection wells close to the power plant or into a nearby surface stream (Zarandi and Ivarsson 2010). In both cases, warm water percolates underground and increases groundwater temperatures. The combination of NNE-trending faults traversing the lava field and the high permeability of the post-glacial lavas controls the distribution of wastewater towards the lake (Zarandi and Ivarsson 2010).

Since the shallow discharge at Nesjavellir geothermal area started 24 years ago, there is evidence of thermal pollution of Lake Thingvellir, which is United Nation heritage site and a sensitive ecosystem with substantial populations of brown trout. In addition, increasing temperatures threaten the aquifer used for the condensate cooling water. To understand and mitigate this problem, a monitoring campaign including tracer testing has been carried out to gain a better understanding of subsurface fluid flow paths. Along with geologic data, monitored temperature and tracer test data are used to calibrate the numerical model presented in this study.

Geologic background

The Nesjavellir geothermal field is situated in a rift valley extending from Hengill to Lake Thingvellir. The area is almost entirely built up of volcanic rocks of late Quaternary and post-glacial age (Árnason et al. 1969), consisting mainly of hyaloclastite

formations erupted during glacial periods and lava flows erupted during interglacial periods. Intrusions dominate at depths > 1 km, and intermediate and felsic rocks are found at depth in many drill holes in the field (Franzson 1988; Franzson et al. 2010).

There are two major sets of normal faults in Nesjavellir associated with the ~ 10 km wide NE–SW-oriented graben structure that runs parallel to the hyaloclastite ridges (Franzson 1988). One fault system is parallel to the NE–SW graben. The other system is oblique to the graben structure, with a strike of N–S that cuts through the valley (Franzson 1988). These faults have an important role in controlling permeability within the geothermal system, as the N–S trending faults appear to act as partial barriers to northeastward flow along the NE–SW structures (Fig. 2a, c). The shallow groundwater aquifers are isolated from the deep geothermal system is isolated from the upper groundwater layers by a low-permeability cap rock layer at ~ 0.5 km depth.

The hydraulic structure of the deep geothermal system in the Hengill area has been investigated in many studies (Bodvarsson et al. 1988, 1993; Franzson 2000; Gunnarsson and Arnaldsson 2011; Gunnarsson and Aradóttir 2014). However, relatively few studies have focused on the shallow part groundwater system above the cap rock. Early studies investigating the subsurface flow patterns through tracer studies (Kjaran and Egilson 1986, 1987) indicated that flow was confined to a rather narrow area between Markagjá in the north and Stapavík in the south, with the core of the flow being situated upwards of the Varmagjá area. Later studies by ÍSOR (Iceland Geosurvey) including a geological model of the area have focused on simulating aquifer response to increased pumping rates or increased reinjection temperature (Hafstað 2000a, b, c, 2001a, b, 2003; Hafstað et al. 2007; Þorbjörnsson et al. 2009; Kristinsson and Hafstað 2011; Kristinsson and Níelsson 2012; Hafstað and Níelsson 2013; Hafstað 2014; Ingimarsson and Hafstað 2015; Ingimarsson et al. 2016; Čypaitė and Ingimarsson 2017; Čypaitė 2018). However, better characterization of the flow paths is needed

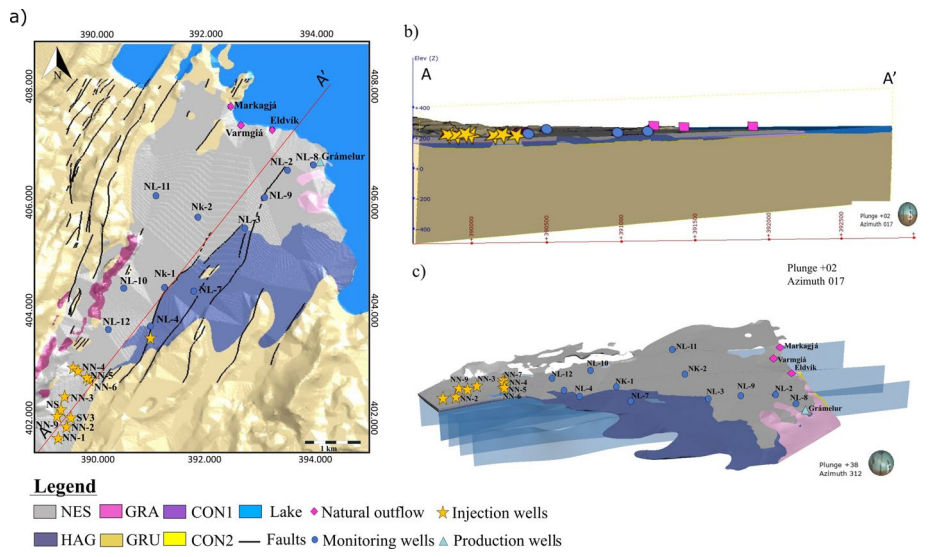

Fig. 2 Map of the Nesjavellir geothermal system. **a** Geological map of the survey area, after Hafstað et al. (2007). **b** Cross-section A–A′ showing major stratigraphic units, Nesjahraun lava flow (NES), Hagavíkurhraun lava flow (HAG), Grámelur cone fragments (GRA) and Grunnberg composite hyaloclastite and lavas (GRU). **c** Detailed view of lava flows and fault planes

to predict the long-term effects of reinjection on the shallow groundwater aquifers and lakeshore.

Methods

Numerical calculations of shallow reinjection and tracer transport were performed with the TOUGH2 simulator (Pruess et al. 1999) and are based on a geologic/conceptual model of the area. Here, we briefly describe the numerical methodology implemented in the TOUGH2 modeling, focusing on the model set-up as well as the tracer and temperature data used to calibrate the numerical model.

Conceptual model development

A three-dimensional geologic/conceptual model of the reinjection zone was developed using Leapfrog Geothermal 4.0 modeling software (Fig. 3). The geologic model incorporates the surface geologic map by Hafstað et al. (2007) and borehole data from nine wells (NK-01, NK-02, NL-04, NL-07, NL-08, NL-09, NL-10, NL-11, NL-12) provided by Reykjavik Energy internal reports. The boundary to the bottom of the model was set to −0.5 km, corresponding to the depth of the deepest injection well NK-5 and the top of the

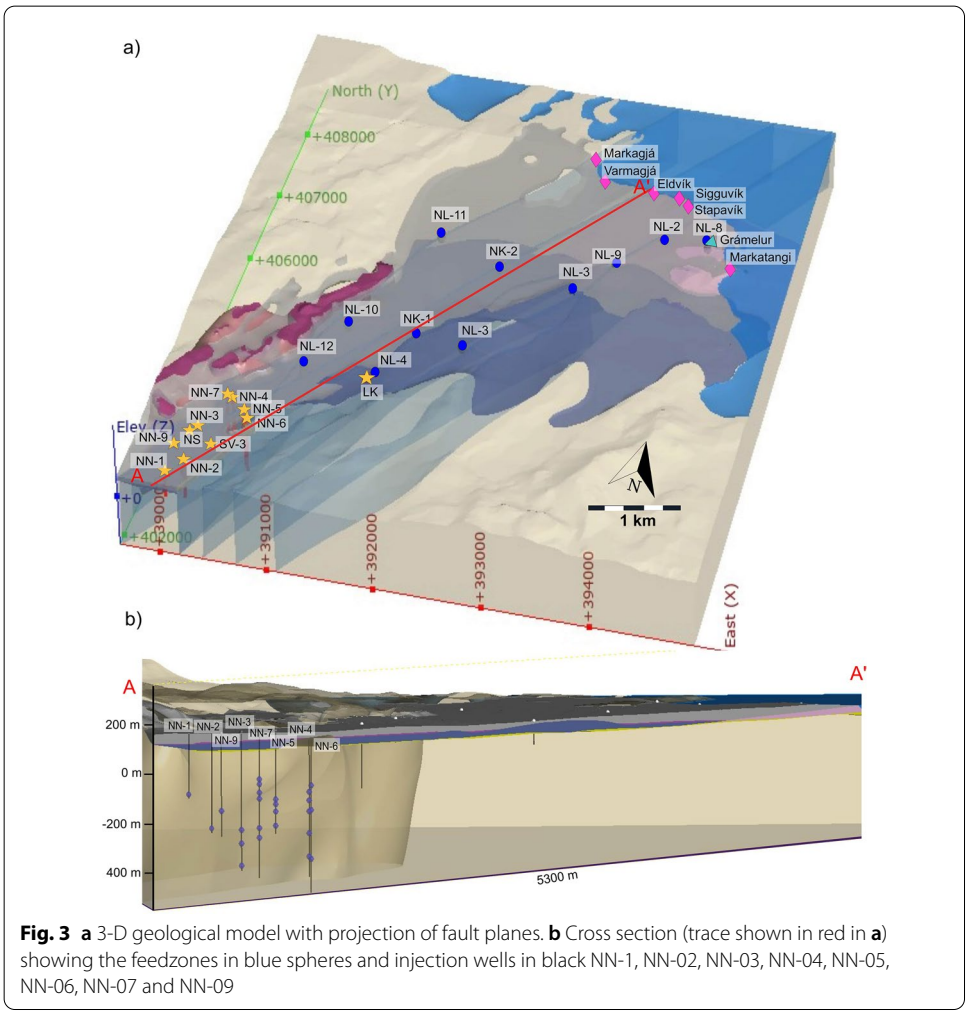

Fig. 3 **a** 3-D geological model with projection of fault planes. **b** Cross section (trace shown in red in **a**) showing the feedzones in blue spheres and injection wells in black NN-1, NN-02, NN-03, NN-04, NN-05, NN-06, NN-07 and NN-09

cap rock. The bedrock lithology according this well is hyaloclastite, as is also observed in other shallow wells, such as NL-02, NL-10, NL-11, NL-07, NL-08 and NL-09. The deeper high-temperature geothermal system, which is mainly located to the south of the power plant, is not included in this model, as it is isolated from the shallow groundwater system by the cap rock.

The subsurface fault system in the Nesjavellir area was modeled based on field mapping (Hafstað et al. 2007) and the results of the tracer test. The faults in the model are near-vertical, with a dip angle between 80° and 90°. The 3D geological/conceptual model of the shallow reinjection area of Nesjavellir geothermal field along with a cross-section cutting the vertical half of the model is illustrated on Fig. 3.

Injection of warm water takes place into deeper injection wells (NN-01, NN-02, NN-03, NN-04, NN-05, NN-06, NN-07, NN-09) and shallow injection wells less than 20 m deep (SV3, LK and NS). The fluid is assumed to enter the system predominantly through the feedzones in each well. The depth of each feedzone for all the wells is shown in Table 1 and projected in Fig. 3b.

Model set-up

Figure 4 shows the computational grid used in this study. The model grid was initially defined using Leapfrog Geothermal, and was refined and optimized in the reinjection area using PyTOUGH (Croucher 2011). The groundwater table data defining the elevation of the upper boundary of the model were obtained from Reykjavik Energy. The thickness of the model is ~ 618 m, ranging between 119.69 masl. to -500 masl., with 19 layers of 45-m thickness and two thinner near-surface layers of 5 and 20 m thickness. The grid extends ~ 7 km in the NE–SW direction and ~ 8 km in the NW–SE direction. The extent of the grid corresponds to the main study area, including the southern part of Lake Thingvellir to the north, hyaloclastite ridges along the eastern and western boundaries, and the location of the power plant to the south. The mesh consists of 22,133 elements with 2396 connections. The grid was rotated by 31° degrees to northeast with the purpose of orienting the grid along an NNE direction parallel to the rift and some of the large NNE–SSW faults. Due to the alignment of the grid with the prevailing strike of many faults, fault-parallel permeability is set to be much higher than cross-fault permeability. Visualization of the grid and model results were performed using Leapfrog and TIM (Yeh et al. 2013).

Table 1 Location and depth of the feedzones in each reinjection well. Reinjected fluid is assumed to be evenly divided between each of the feedzones

Well	Coordinates (x, y)	Feedzone depths (m)	Flow ratio
NN-01	389,994.59 402,110.59	295	1
NN-02	390,119.31 402,298.09	415	1
NN-03	390,105.09 402,777.31	390, 445, 535	1/3
NN-04	390,311.00 403,200.31	280, 300, 330, 388	1/4
NN-05	390,460.00 403,090.00	220, 320, 520	1/3
NN-06	390,450.00 403,081.00	246, 280, 325, 425, 510	1/5
NN-07	390,241.00 403,242.00	200, 220, 255, 280, 400, 440	1/6
NN-09	389,979.00 402,471.00	310	1

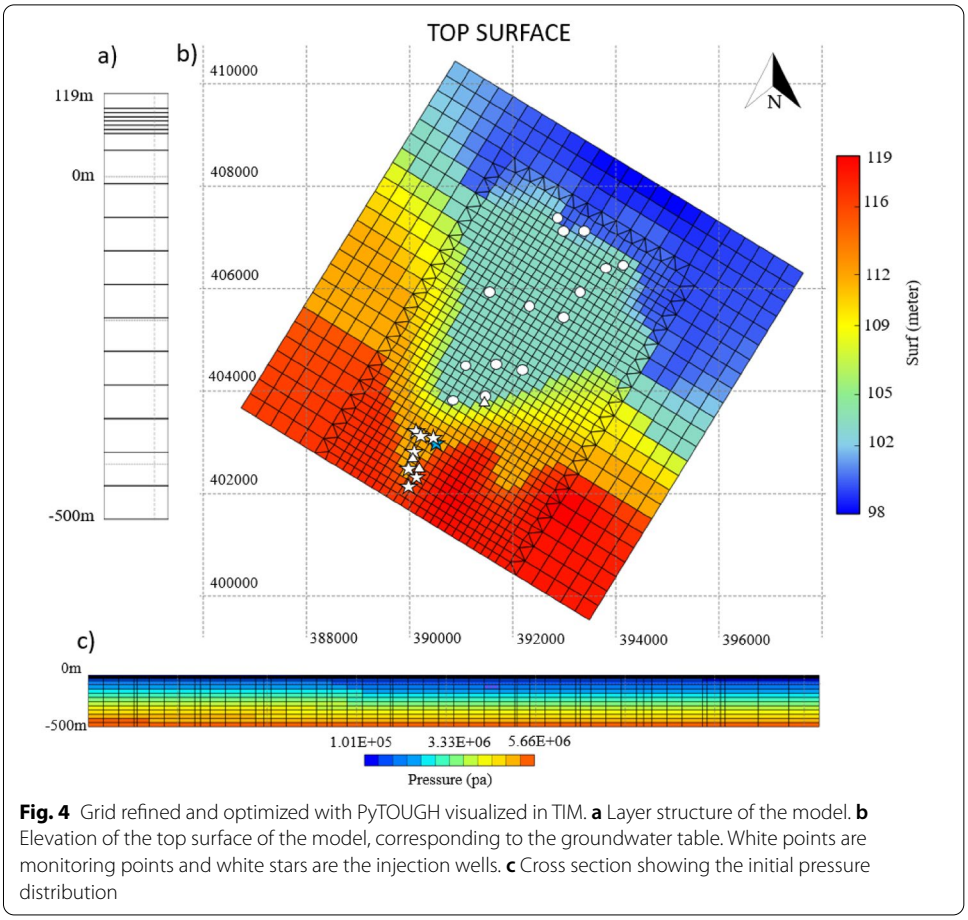

Fig. 4 Grid refined and optimized with PyTOUGH visualized in TIM. **a** Layer structure of the model. **b** Elevation of the top surface of the model, corresponding to the groundwater table. White points are monitoring points and white stars are the injection wells. **c** Cross section showing the initial pressure distribution

The central reinjection zone is modeled using a dual-porosity grid based on the Multiple Interacting Continua (MINC) approach of Pruess and Narasimhan (1985). We considered three interacting continua (one fracture and two matrix blocks) with corresponding volume fractions of 10%—20%—70%, respectively, and a fracture spacing of 100 m. The fracture was assigned a very high porosity (90%). Initially guesses for the hydrological parameters of the main rock types from the geologic model were based on previous modeling studies of the Hengill area (Bodvarsson et al. 1990; Zakharova and Spichak 2012; Snæbjörnsdóttir et al. 2014; Gunnarsson and Aradóttir 2014).

The bottom boundary of the model is fixed at the top surface of the cap rock, which effectively isolates the underlying geothermal system from the shallow groundwater system (Bodvarsson et al. 1988, 1990). Prior to the beginning of reinjection, the majority of shallow wells indicated temperatures near 10 °C. Therefore, the initial temperature in the modeling domain is set to 10 °C. Furthermore, all boundaries are fixed at this temperature. While this potentially neglects addition of heat and mass from the deeper geothermal system, the deep upflow zone of Nesjavellir is located ~ 2 km to the north of the reinjection area (Bodvarsson et al. 1988, 1990; Steingrímsson et al. 2000).

Constant atmospheric conditions are applied over most of the top surface of the model with a fixed pressure of 101,325 Pa. For the columns lying under the water

body hydrostatic pressure corresponding to the depth of the lake (WETB0), where the depth of the lake was based on the bathymetry data retrieved from Stevenson et al. (2012). The numerical simulations are performed in AUTOUGH2 (Croucher and O'Sullivan 2000), a modified version of TOUGH2 (Pruess et al. 1999) developed by the University of Auckland. TOUGH2 uses a fully implicit, integrated finite difference scheme to solve the governing equations of mass and energy conservation. Fluid properties are calculated using equation-of-state module EOS1, which means fluid in the numerical model is assumed to be pure water with properties given by IAPWS-95 (Wagner and Pruß 2002). The EOS1 module is suitable to simulate tracer transport with AUTOUGH2 (Yeh et al. 2012).

Model calibration

The main adjustable parameters in this model are the fracture permeabilities and spatial configuration of the different rock types. Calibration was carried out in two stages. Firstly, the model was calibrated using temperature data collected between 1998 and 2018. Secondly, the model was further calibrated using data from a tracer test performed between November 2018 and September 2019. These two stages are executed in succession, such that the starting temperature distribution in the tracer test is based on the calibrated temperature model. Then, after adjusting permeability structure in order to obtaining a better fit to the tracer data, the temperature model was re-run with the new permeabilities. Thus, model calibration was an iterative process. The model presented below reflects joint calibration of the temperature and tracer data, i.e., with the same geologic structure and identical values for rock permeability in each model.

The temperature data used in the calibration were obtained from internal reports monitored by Reykjavik Energy and ISOR. The natural outflows relevant for this study include Lækjarhvar, Varmagjá, Sigguvík, Markagjá, Markatangi, Eldvík and Gramelur, and temperature in these outflows has been monitored since 1998. In addition, temperature has been monitored on an annual basis in shallow wells NK-1, NK-2, NL-2, NL-3, NL-4, NL-7, NL-8, NL-9, NL-10, NL-11 and NL-12.

The tracer test used to calibrate the simulation involved the injection of 2,7-NDS (naphthalenedisulfonic acid disodium salt) in well NN-6 from November 2018 to September 2019. The average injection rate during the tracer test was 115 l/s, and 100 kg of tracer mass was injected in total. After 30 days of the injection, recovery was detected in NK-1, NK-2, NL-4, and NL-12 wells, with the largest concentration peaks detected in NK-1 and NK-2. There is a second recovery between 70 and 80 days for the natural outflows and NL-2 and possibly a third arrival after 150 days. The location of injection wells, monitoring points and tracer recovery times are illustrated in Fig. 5.

The tracer simulations assume molecular diffusion to be negligible, no phase changes occur in the flow channel and that the mass of the tracer is conserved. As the tracer is injected in relatively shallow groundwaters and not the deeper geothermal reservoir, it is assumed that thermal degradation and chemical reaction of tracer with fluids and rocks in the reservoir does not occur. Nevertheless, not all of the injected tracer is recovered, most likely because some of the tracers could flow into the rock matrix or outside the main flow paths identified in this study.

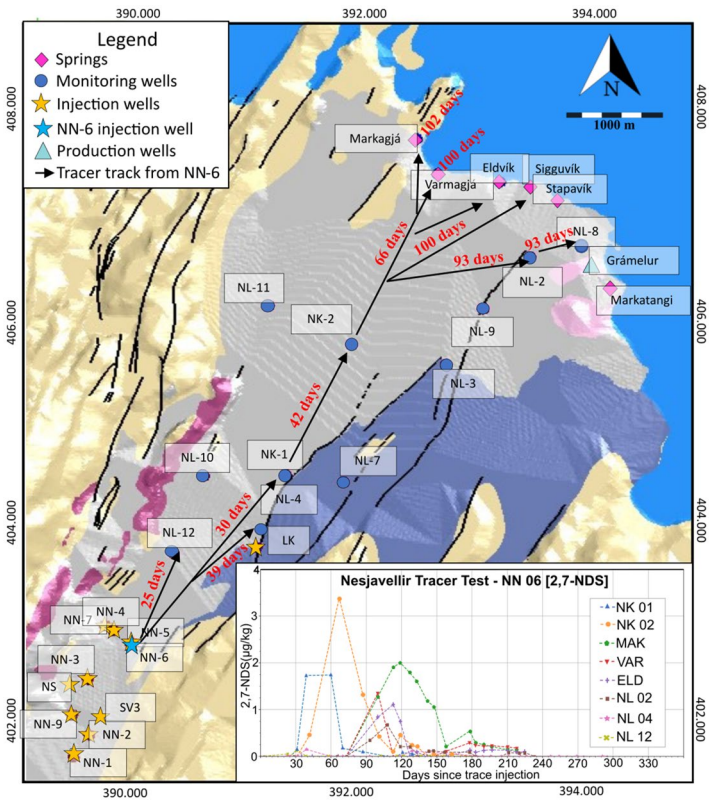

Fig. 5 Tracer test performed in 2018–2019. Injection of 2,7-NDS tracer injected in NN-6 (blue star). Map illustrates the trajectory and measured recovery times of 2,7-NDS between injection and monitoring stations

The injection history from all shallow reinjection wells in the Nesjavellir area is incorporated in the model, since it is the total amount of injected and produced fluid that drives the flow in the system. Figure 6 shows the injection and the discharge rates over the simulation time, as well as the temperature of the discharge water.

The model was refined with the injection and production data for all wells along with the reinterpretation of the structures based on the tracer recovery test from 2018 to 2019. The tracer calibration is a two-component simulation with the second component representing in the tracer into appropriate model wells. The model simulates tracer advection from the 15th of November 2018 until midnight on the 20th of September 2019. Geothermal fluid injection continues in the other wells in the system and data continued to be recorded from monitoring wells during this simulation. In order to keep the steady tracer background value constant and prevent heavy dilution in all injection elements and thus avoid convergence problems resulting from zero values, a miniscule amount of tracer (1×10^{-10} kg tracer per kg injected water) were co-injected within of the injections wells NN-01, NN-02, NN-03, NN-04, NN-06, NN-07, NN-09 and surface injection point Lk during the simulation.

The calibrated model was used to forecast the temperature evolution in response to two end-member scenarios: (i) continued long-term reinjection with injection rate and temperature based on average values for 2018–2019 and (ii) immediate cessation

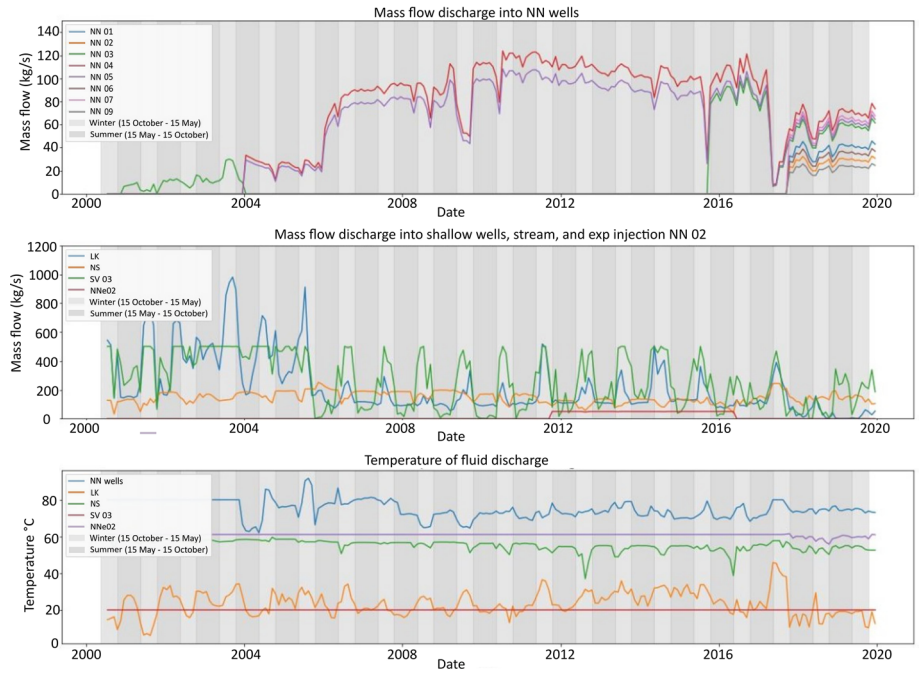

Fig. 6 Total injection rates and temperature of injected water during the simulation time. Dark shades of grey are the winter season and light shades are summer season. NNe02, shown in the middle plot, is an experimental test on NN-02

of the shallow injection. The second scenario considers the amount of time to achieve a steady-state after stopping all the reinjection and production activity in the shallow groundwater field.

Results

Figure 7 shows the geologic structure of the calibrated model. The most important rock types hosting major flow paths are the fault rock types (FAU01, FAU02, FAU03) and the shallow post-glacial lava flows (GRA00, NES00, HAG00). In addition, five rock types were added to the geologic model during manual calibration. Four of these rock types (CHN10, CHN20, CHN30 and FEED0) have very high horizontal fracture permeability ($>10^{-10}$ m^2). CHN10, CHN20 and CHN30 correspond to permeable channels through the lava field at shallow depth (< 50 m), and FEED0 represents permeable zones (layers 10–15 and 17) in the bedrock, as determined by the locations of the feedzones. QDTP0 is a low-permeability layer located to the north of NL-12. The bottom boundary layer (BOUN0) corresponds to the top of the cap rock, and thus has relatively low permeability. Table 2 lists the calibrated fracture and matrix permeability values for the different rock types, as well as the initial rock types in the geologic model with permeability "guesses" based on a literature review.

Temperature model

Figures 8, 9, 10 compare model results (red lines) with measured temperatures (blue lines) in shallow monitoring wells and surface springs located in the reinjection area.

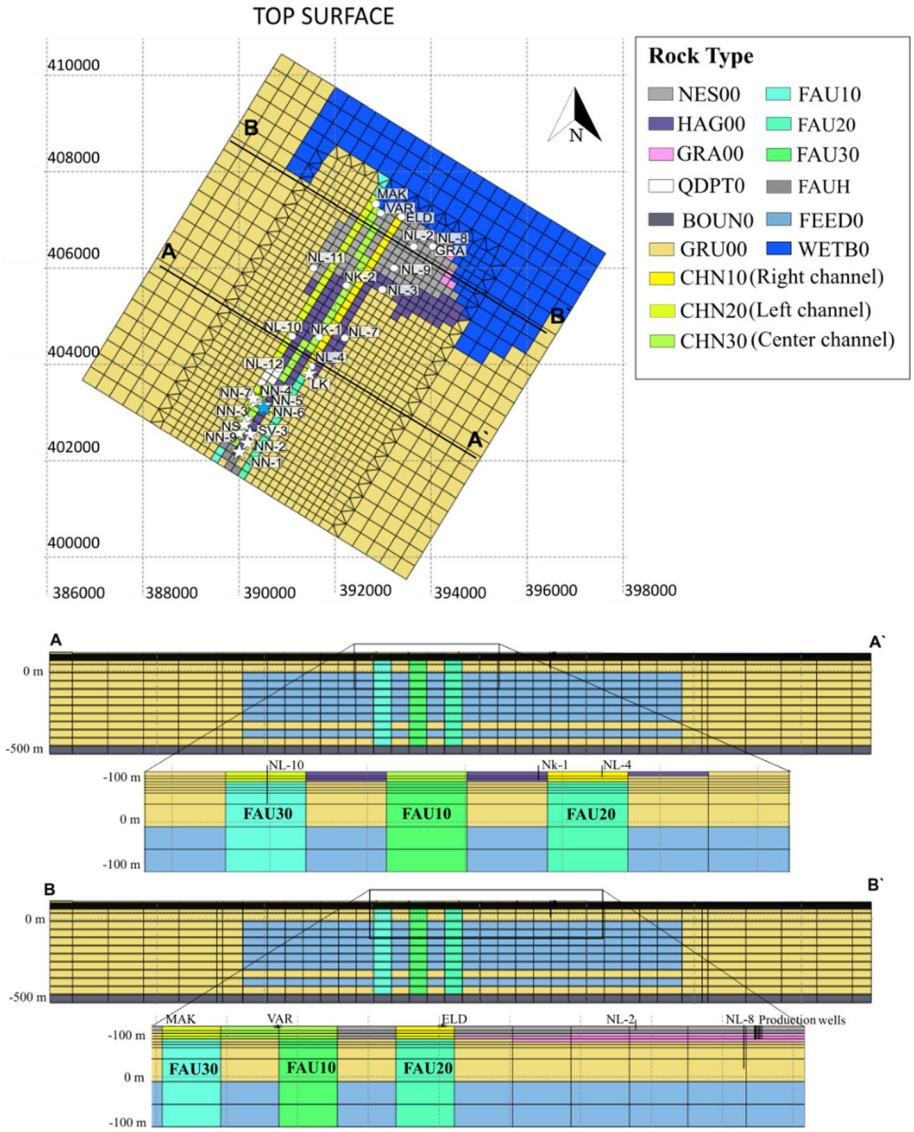

Fig. 7 Calibrated model structure. White stars show injection wells, blue star NN-6 injection well and white points monitoring points. The NS transverse faults are represented by FAU 10, FAU 20 and FAU 30

Temperature has increased by 10–25 °C in the reinjection area over the period 1998–2018. Seasonal fluctuations on the order of ~ 10 °C result from the variable injection of hot water (mass or temperature changes) during different time periods. This is reflected in the model predictions indicating higher groundwater temperatures in the summer, and lower groundwater temperatures in the winter.

The simulation shows a reasonably close match with some of the measured temperature data, reproducing the rate and magnitude of temperature increase in several of the wells. The best matches were obtained for points away from main flow paths, where field measurements indicate temperatures of ~ 10 °C, corresponding to the initial temperature assumed in the temperature model. The models predict a rapid

Table 2 Initial fracture permeability values and rock types based on previous studies (Bodvarsson et al. 1990; Zakharova and Spichak 2012; Snæbjörnsdóttir et al. 2014) and geologic model, and calibrated permeability values with additional rock types illustrated in Fig. 7

Original values				Calibrated values			
ROCK TYPE	Permeability (m^2)			ROCK TYPE	Permeability (m^2)		
	(kx)	(ky)	(kz)		(kx)	(ky)	(kz)
GRA00	$5E10^{-10}$	$5E10^{-10}$	$1E10^{-11}$	GRA00	$1E10^{-09}$	$1E10^{-09}$	$1E10^{-11}$
GRU00	$1E10^{-14}$	$1E10^{-14}$	$1E10^{-15}$	GRU00	$1E10^{-14}$	$1E10^{-14}$	$1E10^{-15}$
HAG00	$1E10^{-13}$	$1E10^{-13}$	$1E10^{-15}$	HAG00	$1E10^{-09}$	$1E10^{-09}$	$1E10^{-15}$
NES00	$1E10^{-13}$	$1E10^{-13}$	$1E10^{-15}$	NES00	$1E10^{-09}$	$1E10^{-09}$	$1E10^{-15}$
FAUH0	$1E10^{-16}$	$1E10^{-16}$	$1E10^{-16}$	FAUH0	$1E10^{-16}$	$1E10^{-16}$	$1E10^{-16}$
FAU10	$1E10^{-12}$	$1E10^{-12}$	$1E10^{-13}$	FAU10	$3E10^{-11}$	$5E10^{-10}$	$5E10^{-13}$
FAU20	–	–	–	FAU20	$3E10^{-12}$	$5E10^{-11}$	$5E10^{-13}$
FAU30	–	–	–	FAU30	$3E10^{-12}$	$5E10^{-12}$	$5E10^{-13}$
BOUN0	$1E10^{-16}$	$1E10^{-16}$	$1E10^{-16}$	BOUN0	$1E10^{-16}$	$1E10^{-16}$	$1E10^{-16}$
				FEED0	$1E10^{-11}$	$1E10^{-11}$	$5E10^{-14}$
				CHN10	$9E10^{-09}$	$9E10^{-09}$	$1E10^{-15}$
				CHN20	$8E10^{-09}$	$8E10^{-09}$	$1E10^{-15}$
				CHN30	$9E10^{-09}$	$9E10^{-09}$	$1E10^{-15}$
				QDTP0	$1E10^{-16}$	$1E10^{-16}$	$5E10^{-16}$

The matrix permeability used for all rock types is $1E10^{-16}$ m^2

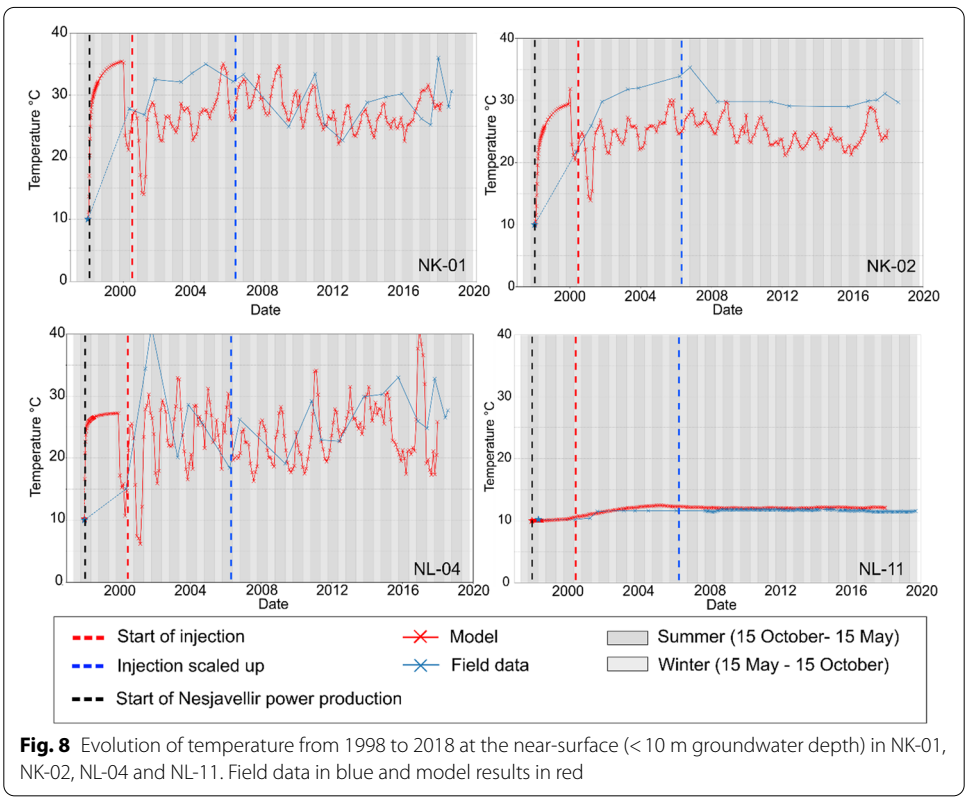

Fig. 8 Evolution of temperature from 1998 to 2018 at the near-surface (< 10 m groundwater depth) in NK-01, NK-02, NL-04 and NL-11. Field data in blue and model results in red

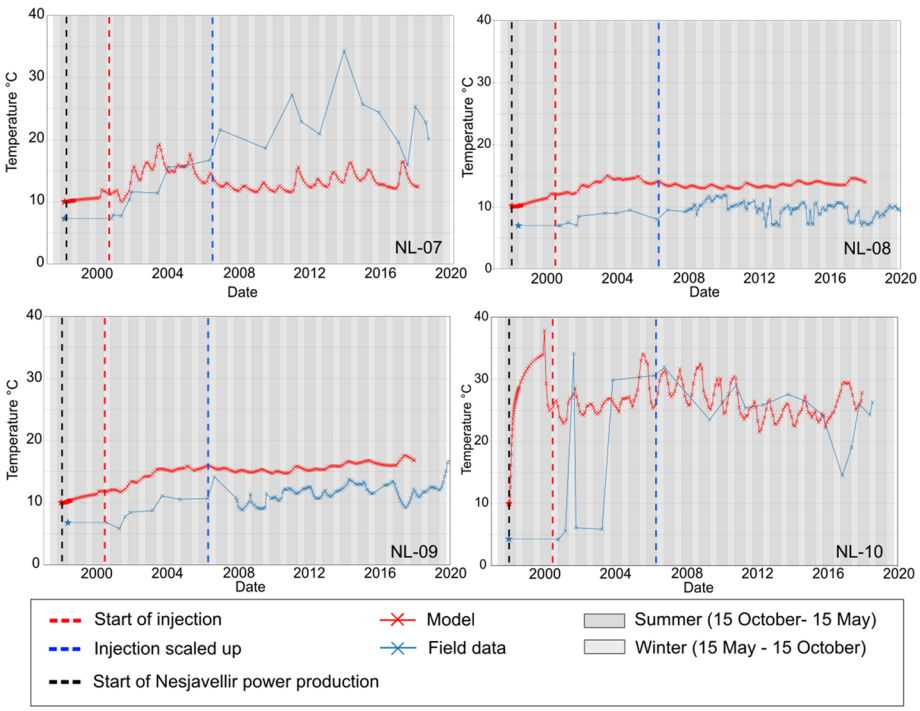

Fig. 9 Evolution of temperature from 1998 to 2018 at the near-surface (< 10 m groundwater depth) in NK-07, NK-08, NL-09 and NL-10. Field data in blue and model results in red

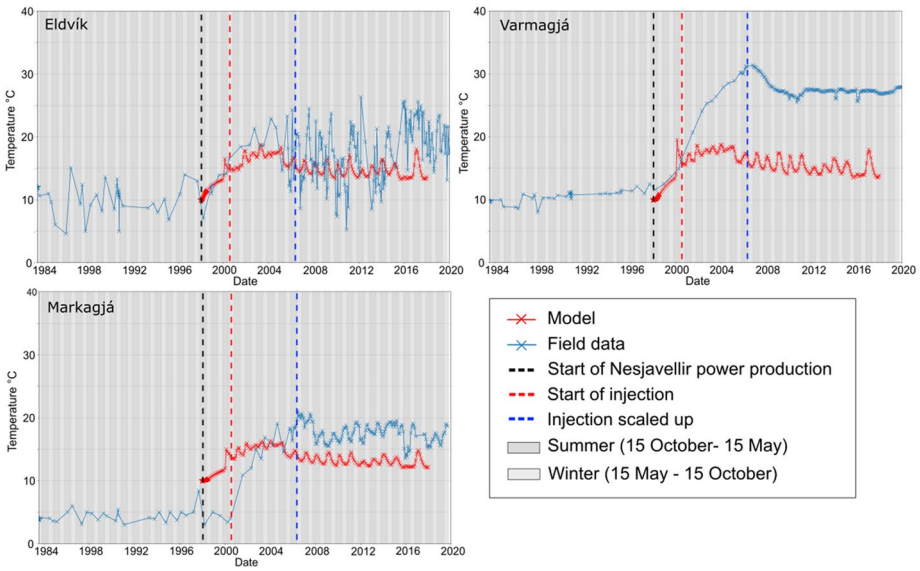

Fig. 10 Evolution of temperature from 1998 to 2018 for springs at 100 masl. Field data in blue and model results in red

increase in temperature during the first 2 years of the simulation period that is not reflected in the measured data (Figs. 8, 9). This potentially reflects elevated resistance to flow (higher viscosity and density) at the onset of the simulation. A better match

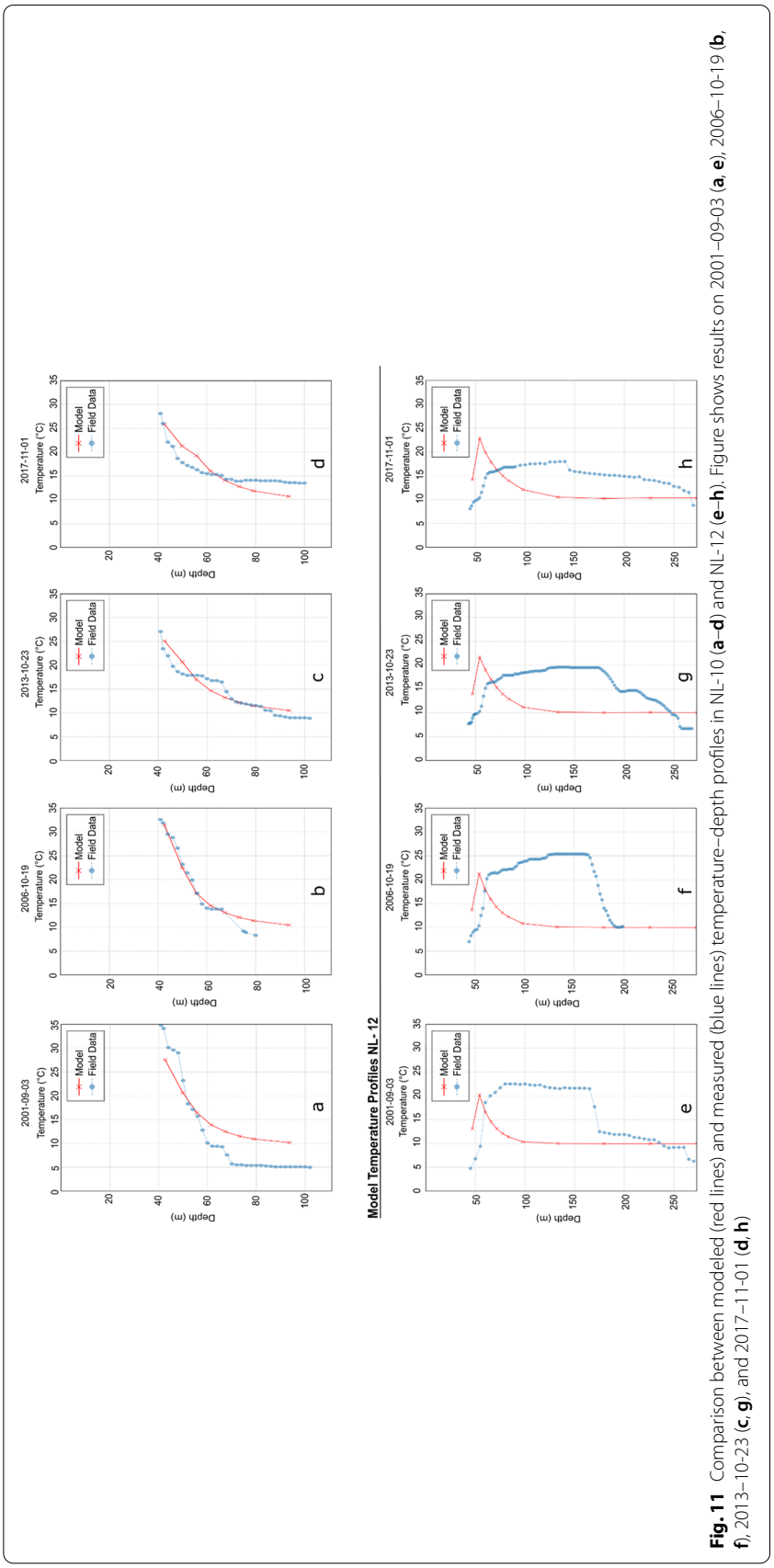

Fig. 11 Comparison between modeled (red lines) and measured (blue lines) temperature–depth profiles in NL-10 (**a**–**d**) and NL-12 (**e**–**h**). Figure shows results on 2001–09-03 (**a**, **e**), 2006–10-19 (**b**, **f**), 2013–10-23 (**c**, **g**), and 2017–11-01 (**d**, **h**)

to the measured data is seen once hydraulic connections to the major structures controlling flow have been established (after the year 2000).

Although shallow monitoring wells such as NK-01, NL-04, and NL-11 (Fig. 8) show a reasonable match to the simulation results, many of the inter-annual fluctuations are not seen in the model results (e.g., temperature increases in 2018 in NL-04, but decreases in the model). In addition, the model underestimates the magnitude of temperature increase seen in NK-02, which reaches up to 35 °C. Certain measurement points (e.g., NL-09, NL-10) indicated initial temperature of 5–8 °C, less than the initial temperature assumed in the model (Fig. 9).

The model underestimates the temperature increase in natural outflows (Fig. 10). Eldvík shows seasonal variations in temperature, the model predicts a lesser amplitude of seasonal variability than measured (Fig. 10a). For Markagjá, the model predicts a lower rate and magnitude of temperature increase than measured, resulting in ~ 5 °C discrepancy. Although data suggest the greatest temperature increase in Varmagjá, the models predict a similar magnitude of temperature response as the other natural outflows, resulting in a 10–13 °C discrepancy between the model and the field data.

In addition to the temperature transients presented in Figs. 8, 9, 10, temperature–depth relations were used to calibrate the model. Figure 11 shows the temperature–depth profiles for NL-10 (top panel) and NL-12 (bottom) at four different times between 2001 and 2017. The simulations reproduce the overall temperature gradient in NL-10 (Fig. 11a–d), but do not reproduce the temperature increase at > 60 m depth. The simulations also predict a sharper temperature inversion in NL-12 (Fig. 11e–f), the deepest monitoring station. However, the field data indicate a warm plume between 60 to 160 m depth that first increases and then decreases in magnitude over the simulation period. Other stations such as NK-01, NK-02, NL-04 and NL-07 showed measurements over restricted depths (< 5 m) but reasonable matches through 20 years, with a slight difference and discrepancy on certain dates.

Heat transport is controlled by the shallow high-permeability post-glacial lava flows in the near-surface, as well as major rift-parallel faults (FAU01, FAU02, FAU03), which transport heat advectively from reinjection to the NE along the rift. Figures 12, 13, 14 compare the temperature distribution in the lava field at ~ 100 masl. (layer 1) with isotherm maps generated by ÍSOR for September 2000, October 2006 and May 2017. Soon after the beginning of shallow reinjection (Fig. 12), a plume with temperatures 20–40 °C develops along the most permeable fault (FAU10). Temperatures along this fault are most elevated in the uppermost, high permeability, lava flows. Temperature remains unchanged at greater depths since the injection of warm water at deep levels has not yet started. The simulation illustrates that temperature increases most rapidly in the NE–SW, reaching 30 °C in the center of the field and 15–20 °C close to the lake, a good overall match to the field data. In addition, the simulations reproduce the bending of the thermal plume towards the east along the shore of Lake Thingvellir.

By October 2006 (Fig. 13), temperature has increased to ~ 20 °C throughout most of the lava field, with the area between the 20 °C and 30 °C isotherms extending to the lake. After deep reinjection at depths 0–0.5 km, simulated temperature is 60 °C close to the deep injection wells (NN-3, NN-4 and NN-5). However, this deeper thermal plume extends a shorter distance to the NE compared to the thermal plume in

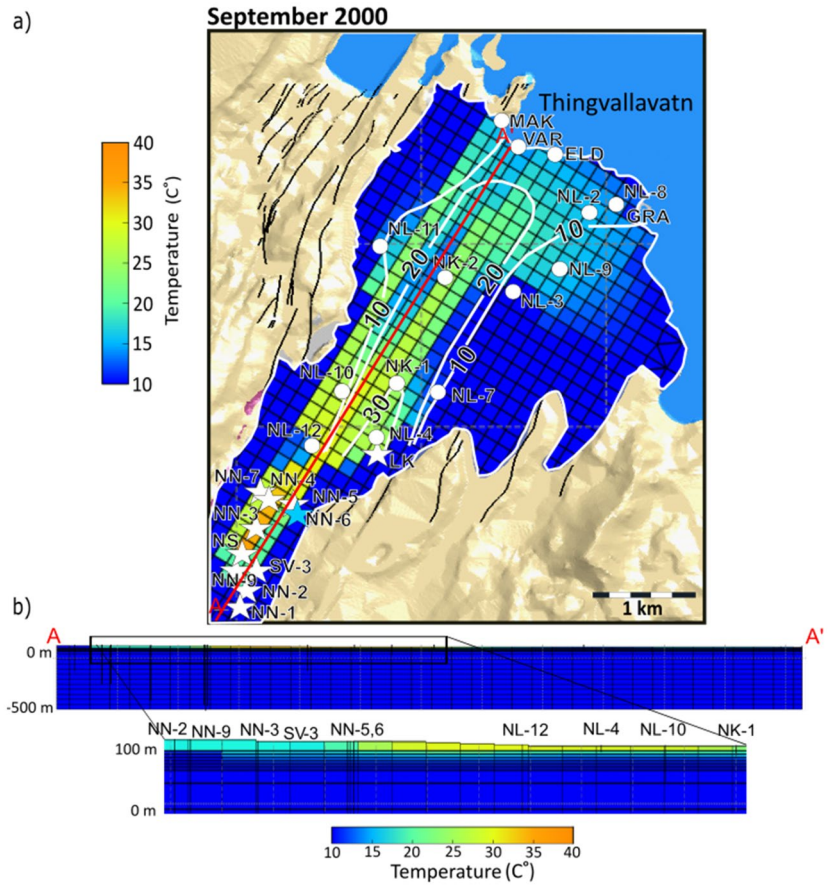

Fig. 12 **a** Comparison between measured temperature at one meter below the groundwater table for September 2000. The contour lines represent the temperature registered from ÍSOR data. White dots are the monitoring station, white stars are the injection wells and blue star is the injection well NN-6 chosen for the tracer test. **b** Cross section along the most permeable fault (FAU10)

the shallow lava flows. The simulation shows a low-temperature area (15 °C) between NK-02 and NL-11. Although there is a lack of monitoring data in this area to confirm these predictions, the cooler temperatures are the result of a lower permeability. As result of this separation, interactions between the warm flows in faults FAU01–FAU03 are limited.

By May 2017 (Fig. 14), temperature has increased to ~ 30 °C in the permeable channels, especially along the injection well to NK-02 and along the edge of the lake. However, the temperature has increased over a significant area of the lava field, mainly with a northeast trend seen in the field data as well as simulation results. It is observed that between CHN20 and CHN30 there is a cold water zone, but this is due to between NL11 and NK2 there is no record of measured data and no permeable channel was made between them. At deeper levels, the simulated temperature has increased to 30–40 °C over a large vertical interval in the subsurface and extends ~ 3–4 km to the NE along the main rift-parallel fault. The bend in the thermal plume to the west in the vicinity of Lake Thingvellir is clearly visible, although the model predicts somewhat higher temperatures (up to ~ 20 °C) extending 1 km further to the SW.

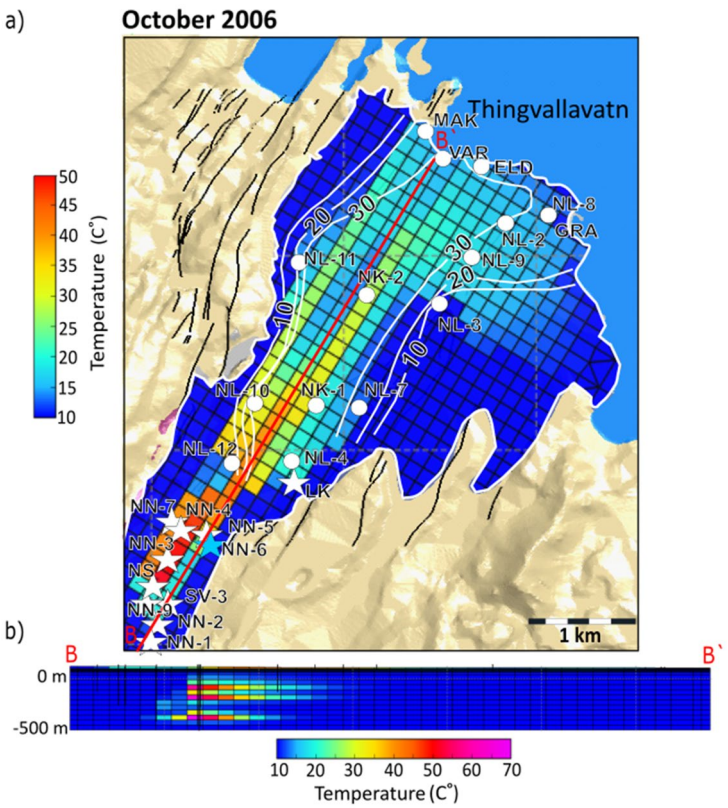

Fig. 13 **a** Comparison between temperature ÍSOR map and simulation for October 2006. White dots are the monitoring station, white stars are the injection wells and blue star is the injection well NN-6 chosen for the tracer test. Groundwater temperature one meter below the groundwater table. **b** Cross section along the most permeable fault (FAU10)

Figure 15 compares simulated temperature with temperature calculated using isotherm maps based on groundwater temperature data acquired between 2018 and 2019. The temperature distribution calculated using the isotherm maps was generated in Leapfrog using an RBF interpolant method. These results show the broad zone with temperature > 50 °C around the deep injection wells in the SE (cross-section A–A′, Fig. 15b). To the NE (cross-section B–B′, Fig. 15c), elevated temperatures become increasingly confined at depths < 0.1 km, and the highest temperatures are found along the main permeable fault. The simulations predict a more extensive area of elevated temperature spread out to the southeast in the near vicinity of the lake (Fig. 15).

Tracer calibration

Tracer advection is controlled by the shallow high-permeability lava flows at shallow depths and the SW–NE oriented fault at greater depths. Figure 16 shows the tracer distribution at 86 masl. (Fig. 16a–d) and − 180 masl. (Fig. 16e–g). The simulations predict a relatively broad (~ 0.5 km) plume of tracer within the shallow lava flow. This plume migrates to the NE, and after 42 days reaches the shore of Lake Thingvellir. After 126 days, the highest tracer concentrations in the shallow lava flow are confined to the area in the near vicinity of the lake. At greater depths (Fig. 16e–g),

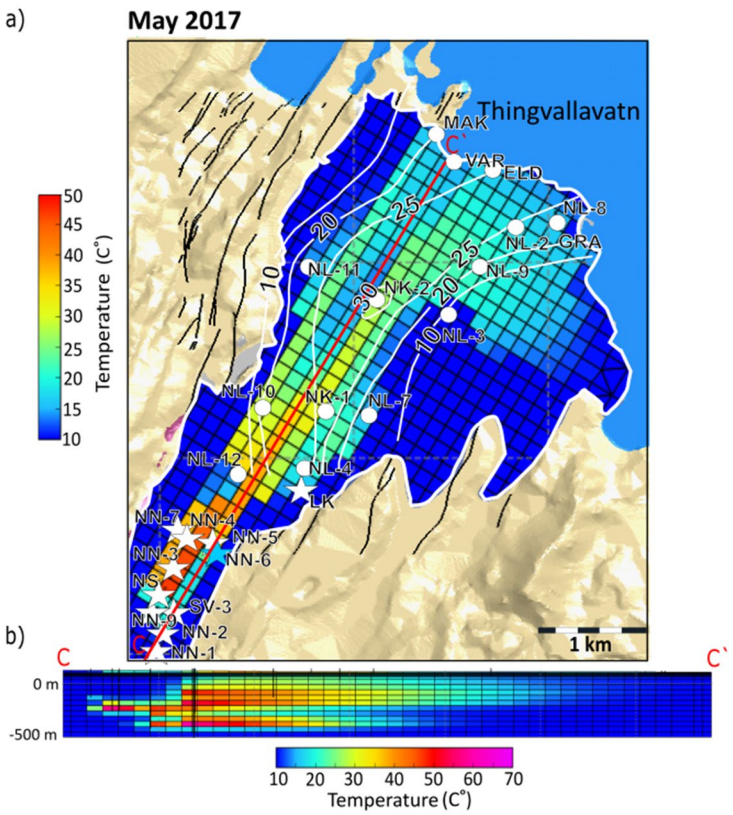

Fig. 14 **a** Comparison between temperature ÍSOR map and simulation for May 2017. White dots are the monitoring station, white stars are the injection wells and blue star is the injection well NN-6 chosen for the tracer test. Groundwater temperature 1 m below the groundwater table. **b** Cross section along the most permeable fault (FAU10)

tracer concentrations are significantly elevated along the main NE–SW-oriented fault. While tracer concentrations are greater at depth within the fault compared to the shallow lava flow, the anomaly is not as broad.

Model results show reasonable agreement with some of the field data collected during the tracer test in 2018–2019. The simulations reproduce the overall arrival time, peak tracer concentration and shape of the measured tracer return curves in several of the monitoring stations, particularly NK-01 and NK-02 (Fig. 17a,b). The field data record a more rapid tracer return in the natural outflows Varmagjá, Eldvík and Markagjá compared to the simulations (Fig. 17c–e). In the wells NL-02 and NL-04, the modeled and measured tracer concentration peak is similar, but the simulations suggest a relatively broad peak compared to the narrow peak measured in the field data (Fig. 17f,g). The simulations predict no tracer arrival in NL-12, although very low concentrations were measured (Fig. 17g).

Table 3 summarizes the main observations from the field temperature/tracer data and the corresponding calibration results.

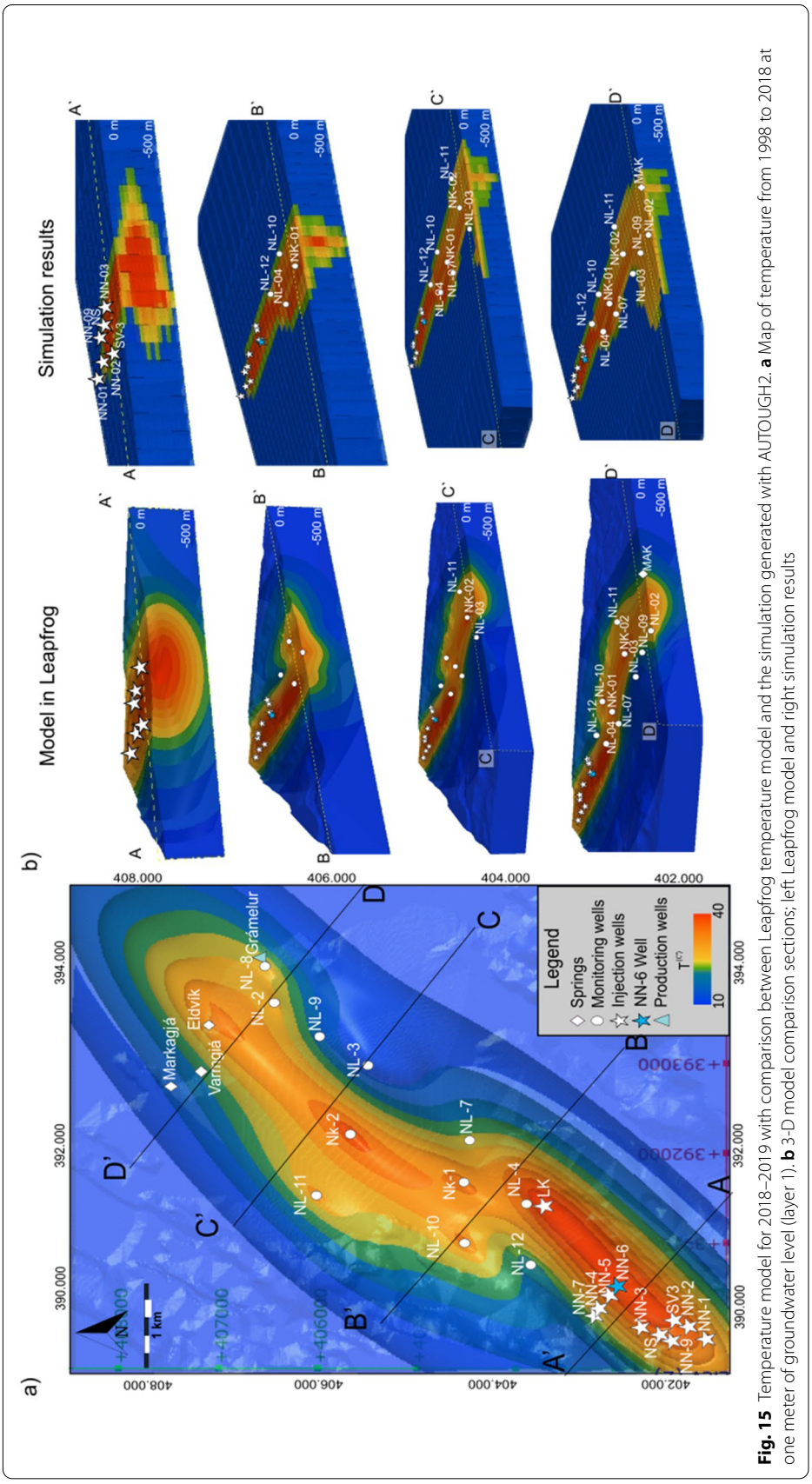

Fig. 15 Temperature model for 2018–2019 with comparison between Leapfrog temperature model and the simulation generated with AUTOUGH2. **a** Map of temperature from 1998 to 2018 at one meter of groundwater level (layer 1). **b** 3-D model comparison sections; left Leapfrog model and right simulation results

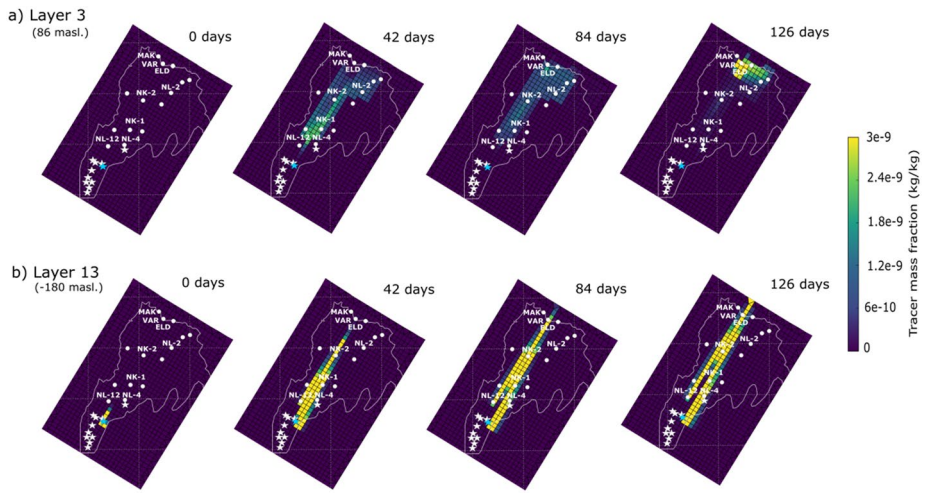

Fig. 16 Model results for tracer test performed in 2018–2019. The results are shown at a different time intervals of 0 day, 42 days, 84 days and 126 days for layer 3 (**a**) and layer 13 (**b**)

Future scenarios

Two different future scenarios were evaluated using the calibrated model starting from 2020. In the first scenario, shallow and deep reinjection continues for 20 years with the same injection rate and temperature as used during the period 2018–2019 (Fig. 18). In the second scenario, all reinjection is stopped across the reinjection area (Fig. 19).

After 10 years of continued reinjection, temperature at 86 masl (near the surface) increases slightly close to the edge of the lake but more strongly at depth along the main fault, with temperature increases up to 45 °C and 60 °C at 86 masl and -180 masl, respectively. After 20 years, most of the shallow lava field has temperatures > 25 °C, with values close to 35–40 °C in the main channels and 30 °C close to the lake. At 86 masl., the maximum temperature is around 60 °C, with temperatures around 50 °C in the main channel and 40 °C in the Grámelur area. At depths of -180 masl., the zone of elevated temperature (60 °C) reaches the shoreline. The vertical cross sections along the most permeable fault highlight the increasing temperatures with time.

In the second scenario (Fig. 19), temperature drops rapidly on the surface and more slowly at depth. After 10 years, the shallow temperature is 12–13 °C, close to the initial temperature prior to the beginning of reinjection. At greater depths, temperatures > 30 °C persist in the area surrounding the injection zone and along the main channel, but the area closer to the lake cools rapidly.

Discussion

Hydraulic structure of the reinjection area

Heat and fluid transport in the Nesjavellir shallow reinjection zone is controlled by the heterogeneous permeability structure. The model illustrates that NNE-trending rift-parallel normal faults act as flow paths that channel the fluid from the injection zone to the northeast. At shallow depths (< 0.1 km), reinjected fluid spreads out within the

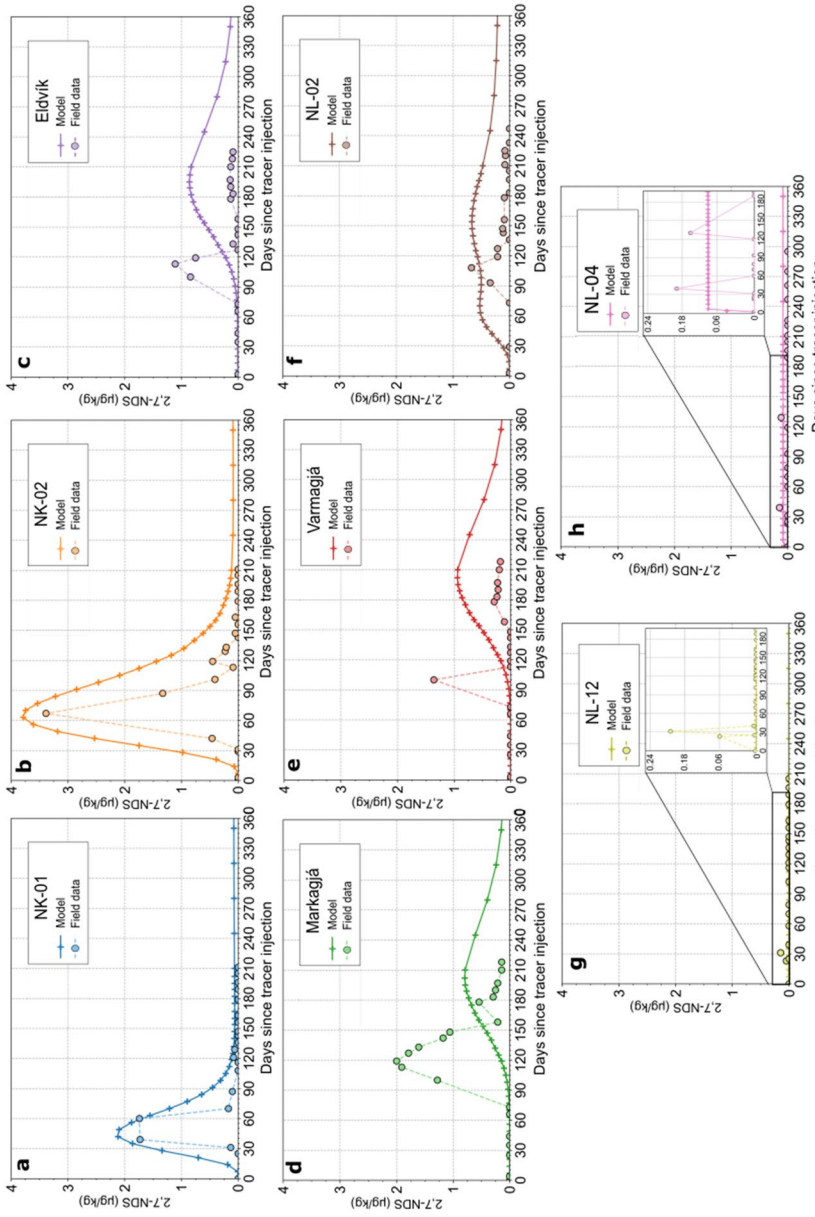

Fig. 17 Comparison of model-predicted tracer return curves with measured data in **a** NK-01, **b** NK-02, **c** Eldvík, **d** Markagjá, **e** Varmagjá, **f** NL-02, **g** NL-12, and **h** NL-04. The field data are represented by the dots and the dotted line, and the model results by the plus sign symbol and the solid line

Table 3 Major characteristics observed by the field data and calibration results

Major characteristic observed	Calibration results
Rate and magnitude of temperature increase at shallow depth in shallow monitoring wells (Figs. 8, 9)	Model overestimates initial rate of temperature increase. Long-term magnitude of temperature increase matched in NK-1, NL-4, and NL-10. Slightly underestimates temperature increase in NL-02 and NL-07. Overestimates temperature increase in NL-08 and NL-09
Temperature increase measured at shallow outflows along lake (Fig. 10)	Model reproduces temperature increase at Eidvik but underestimates seasonal fluctuations. Slightly underestimates rate and magnitude of temperature increase at Markagja and strongly underestimates magnitude of temperature increase at Varmagja
Temperature–depth relations in shallow monitoring wells (Fig. 11)	Model reproduces temperature reversals in NL-10 resulting from shallow outflow along lava flow. Warmer isothermal zone between 50 and 150 m in NL-12 is not present in model results
Tracer return time in shallow monitoring wells and natural outflows (Fig. 17)	Rapid returns in NK-1 and NK-2 reproduced. Model predicts later tracer return than observed in natural outflows
Shape of the tracer return curve (Fig. 17)	Model reproduces narrow peak in tracer return curve in nearby monitoring wells. Model prediction of long-tail (higher tracer concentrations at later times) in natural outflows not observed in measured data

post-glacial lava flows extending to the shores of Lake Thingvellir. The recorded temperature and the tracer test observed in the field data suggest the presence of fracture flow channels in the lavas connecting mainly the NK-1, NK-2 wells and the Varmagjá, Eldvík and Markajía springs with the area of injection. The NNE-trending faults near NN-6 functions as the main flow path, where it in turn cuts the lavas at the surface, generating a further increase in permeability. However, even though the faults are parallel, the shallow channels have a more irregular structure and several of them may join with each other or with other unidentified permeable structures. In addition, the presence of undetected vertical and/or transverse faults at depth could also play a role in heat and mass transport. Calibration results suggest that the fault zones and shallow lava flows have very high horizontal fracture permeability ($\sim 10^{-10}$ m^2) and moderate vertical fracture permeability ($\sim 10^{-15}$ m^2). At depths between -100 and -400 masl, the injected hot fluid flows laterally through the vertically oriented fault damage zone. Lithologies that bound this fault zone at depth do not host large-scale flow of the injected fluid.

The temperature rise in the permeable channel between NK-01 and NK-02 suggests that the flow was concentrated in a narrow path between the injection and the monitoring wells, as seen in the tracer test. The spread out of the temperature increase near the immediate vicinity of the lake around Grámelur results from the permeable lavas that help dissipate the flow. Although the simulations suggest a migration of injected fluid towards the east at the edge of the lake, this cannot be verified since there is no monitoring data available in this area. While the model results in an acceptable match between the simulated tracer return curve and the actual tracer return profile for NK-01 and NK-02, the peak tracer concentration in NK-01 was not recorded the measured data (i.e., the peak occurred somewhere between 40 and 60 days after tracer injection, when no sample was collected), and it is possible the

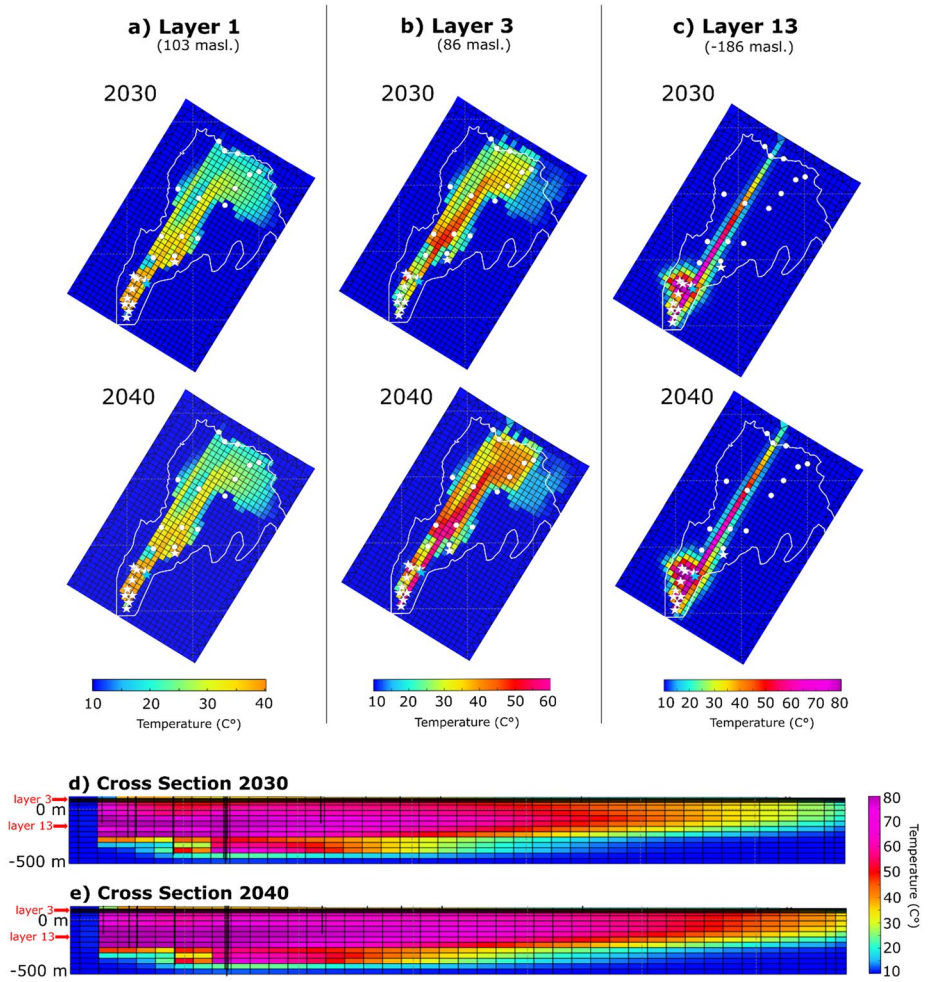

Fig. 18 Evolution of temperature in 2030 and 2040 if injection and production continue at the same average flow rate and temperature from 2018 to 2020 observed in layer 1 (**a**), layer 3 (**b**) and layer 13 (**c**). Cross section along the most permeable fault (FAU10) for 2030 (**e**) and 2040 (**d**)

model underestimates the strength of the hydraulic connection between NN-06 and NK-01. More troublingly, the model does not accurately reflect the tracer recovery curves at the natural outflows. This may indicate that rock permeability closer to the lake may be underestimated, or that the degree of flow channeling is underestimated.

Implications

Thermal pollution of Lake Thingvellir poses an environmental risk to an important ecosystem. If shallow reinjection in the shallow lava flow and in the vicinity of the NNE-trending fault zone continues, the models suggest the potential for further temperature increases near the lake. While the models suggest that the maximum temperature in the surface outflows will be ~ 35 °C, temperatures up to 50–60 °C will occur around 2040 at ~ 20 m depth. Although studies have suggested that thermal pollution can have varied and localized effects on aquatic invertebrates in Lake Thingvellir (Snorrason et al. 2011), such temperature increases are may lead to

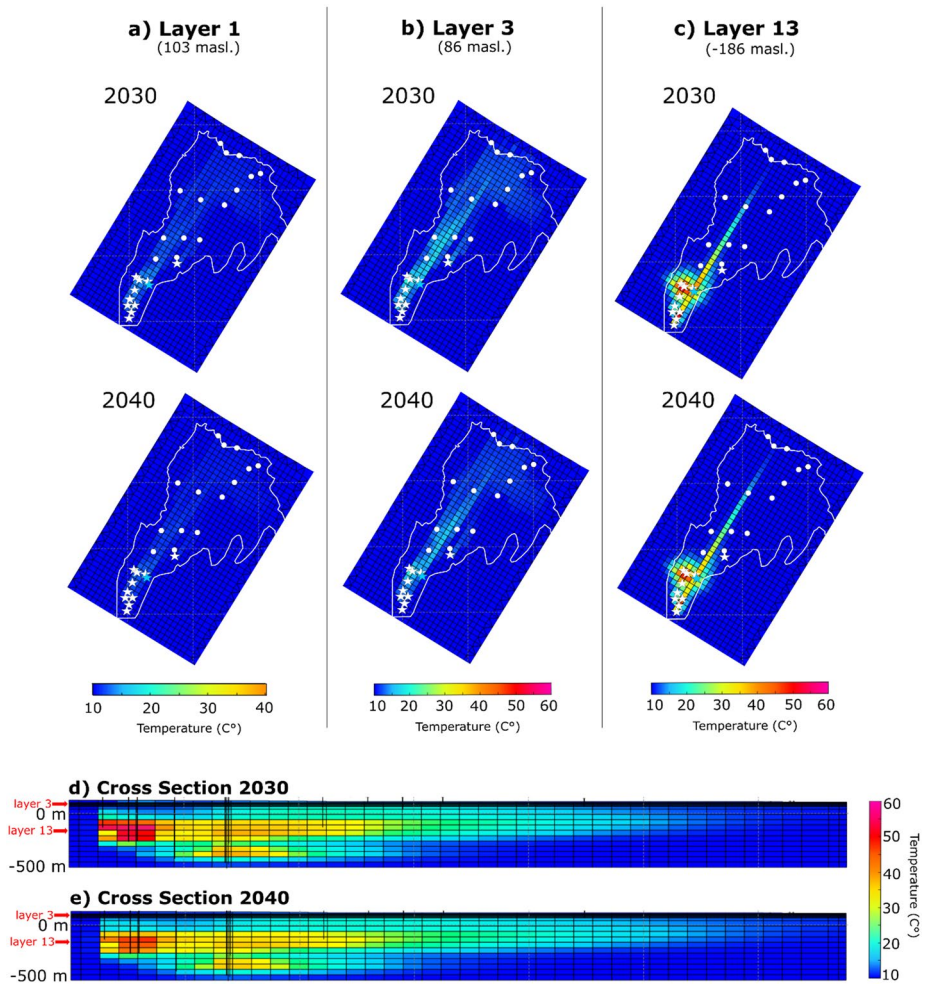

Fig. 19 Evolution of temperature for 2030 and 2040 if all injection and production is stopped in layer 1 (**a**), layer 3 (**b**) and layer 13 (**c**). Cross section shows temperature distribution along the most permeable fault (FAU10) for 2030 (**d**) and 2040 (**e**)

unacceptable environmental impacts, thus requiring modification of the reinjection strategy. Encouragingly, the models show that if reinjection ceases in this zone, temperatures near the lake will recover to values ~ 10 °C within 10 years, close to what was measured prior to the onset of injection.

The practice of discharging separated brine and condensed steam into shallow wells or surface waters has become increasingly uncommon in the geothermal industry. Zarandi and Ivarsson (2010) suggested several alternative measures to reduce the effects of thermal pollution in Lake Thingvellir, including increase the size of the cooling tower, drilling deep reinjection wells, or relocating the discharge area to the western part of the valley. Already the current reinjection strategy at Nesjavellir has been adjusted in recent years, with the commencement of reinjection into well NJ-18 on the northwestern edge of the field (Gunnarsson et al. 2020). We suggest continued adoption of such measures will help avoid further thermal pollution of the lake.

Future improvements to model

Natural outflows of geothermal fluid at the surface are neglected in the presented model, which assumes an initial temperature of 10 °C throughout the modeling domain and fixed temperatures of 10 °C at all boundaries. Perhaps as a result, the model fails to reproduce certain aspects of the measured data (Table 3), and in particular underestimates the magnitude of temperature increase and tracer recovery time in natural outflows. The springs in Varmagjá showed somewhat elevated temperatures prior to injection (Fig. 10), which has been interpreted as indicating a geothermal signature potentially resulting from runoff from the natural geothermal springs and fumaroles at the Nesjavellir geothermal field (Zarandi and Ivarsson 2010). Therefore, better incorporation of natural geothermal input into the field is needed, and could be obtained by running initial simulations that match the steady-state temperature distribution in the reinjection area. In addition, the model could be coupled with the larger-scale fluid flow model developed for the Hengill area (Gunnarsson et al. 2011) to better constrain heat and mass flows across the impermeable cap rock at the base of the shallow reinjection area.

In addition, further refinement of permeability structure near the lake shore is needed to improve the match time recovery for the natural outflows. The permeability in this area could be increased, or the degree of channelization enhanced, in order to reproduce the more rapid tracer recovery in this area. Additionally, seven other tracers were injected in the system during the tracer test in 2018–2019. Calibrating the model for each tracer as was done in this study would improve the understanding of the flow paths, especially the area near the lake within the lava flow Nesjahraun, which was not possible to characterize very well using the data presented here. In addition, further experimentation with other parameters for the dual-porosity model (e.g., matrix fraction and porosity values) could improve the match between measured data and simulation results. Although the model should be recalibrated to obtain a better fit, even under its current state, it shows the potential to be useful for shallow injection management and forecasting.

Conclusions

This study presents a numerical model of the shallow reinjection zone in the Nesjavellir geothermal field. The numerical model is calibrated using long-term (20+ years) temperature monitoring data and results from a tracer test performed in 2018–2019. The numerical model reproduces the 10–25 °C temperature increase within the shallow high-permeability post-glacial lava flows. At greater depths, flow is largely confined to two rift-parallel faults extending between the Nesjavellir reinjection zone and Lake Thingvellir. The model calibration results indicate very high horizontal fracture permeability (10^{-10} m^2) in the fault rock types and post-glacial lava flows. While the model generally reproduces the measured tracer recovery and peak for the monitoring stations, the temperature and tracer calibration for natural outflows could be improved.

Given that the temperature and the tracer simulation match the field data with the selected hydrological parameters, the model shows that it is possible to make a forecast on the possible behavior of the system. With continuous injection, the temperature after

20 years will be around 35 °C for shallow levels (− 90 masl.) and higher than 50 °C for intermediate and deeper levels below lava flow limited with the Lake Thingvellir. In the event that the injection is ceased, the temperature will be close to initial condition shallow levels around all the lava flow field, especially near Lake Thingvellir, after only a few years. Although the area around the deeper injection zone may take more than 20 years to cool down, this will pose comparatively little risk to the ecosystem at Lake Thingvellir.

Acknowledgements
The authors thank Reykjavik Energy (OR) for providing valuable data, assistance, and support during this research. Due to the nature of this research, and the data policy of the entity that owns the dataset, the supporting data are not available for sharing publicly.

Author contributions
EG-D constructed the 2D maps, 3D geological model and set up the numerical model with the assistance of TR. EG-D conducted the calibration and simulations, and wrote the manuscript with the collaboration of SS. All authors participated in the interpretation of the numerical simulations and enhances to the numerical model and discussion of general results. SS and JN participated in a significant part in the revision of the manuscript and contributed to every aspect of the study. TR and SS supported in large part with improving the code script throughout the research. All authors read and approved the final manuscript.

Funding
Open Access funding enabled and organized by Projekt DEAL. Open Access funding enabled and organized by Projekt DEAL. The research received no specific grant from any funding agency in the public, commercial, or not-for-profit sectors.

Availability of data and materials
The data that support the findings of this study are available from Reykjavik Energy (OR) but restrictions apply to the availability of these data, which were used under license for the current study, and so are not publicly available. However, the data are available from the authors upon reasonable request and with the permission of Reykjavik Energy (OR).

Declarations

Competing interests
The authors declare that they have no known competing financial interests or personal relationships that could have appeared to influence the work reported in this paper.

Author details
[1]Energy and Minerals Resources Group, Geological Institute, RWTH Aachen University, Wüllnerstraße 2, 52056 Aachen, Germany. [2]Iceland School of Energy, Reykjavik University, Menntavegur 1, 102 Reykjavik, Iceland. [3]University of Iceland, Sæmundargata 2, 102 Reykjavik, Iceland. [4]Carbfix, Bæjarháls 1, 110 Reykjavík, Iceland.

Received: 16 October 2021 Accepted: 1 April 2022
Published online: 27 April 2022

References

Árnason B, Theodorsson P, Bjornsson S, Saemundsson K. Hengill, a high temperature area in Iceland. Bull Volcanol. 1969;33:245–160. https://doi.org/10.1007/BF02596720.
Axelsson G. Tracer tests in geothermal resource management. EPJ Web Conferences. 2013;50:02001. https://doi.org/10.1051/epjconf/20135002001.
Axelsson G. Importance of geothermal reinjection. In Proceedings: Workshop for Decision Makers on the Direct Heating Use of Geothermal Resources in Asia, UNU-GTP, TBLRREM and TBGMED, Tianjin, China, 2008.
Axelsson G. Role and management of geothermal reinjection. Short Course on Geothermal Development and Geothermal Wells", organized by UNU-GTP and LaGeo, Santa Tecla, El Salvador, 2012.
Bodvarsson GS, Bjornsson S, Gunnarsson A, Gunnlaugsson E, Sigurdsson O, Stefansson V, Steingrimsson B. The Nesjavellir Geothermal Field, Iceland, Part I. Field characteristics and development of a three-dimensional numerical model. Geothermal Sci Technol. 1990;23:189–228.
Bodvarsson GS, Bjornsson S, Gunnarsson A, Gunnlaugsson E, Sigurdsson O, Stefansson V, Steingrimsson B. Summary of Modeling Studies of the Nesjavellir Geothermal Field, Iceland. In: Proceedings: 13th Workshop on Geothermal Reservoir Engineering, Stanford University, CA, USA. 1988.
Bodvarsson GS, Gislason G, Gunnlaugsson E, Sigurdsson O, Stefansson V, Steingrimsson B. Accuracy of Reservoir Predictions for the Nesjavellir Geothermal Field, Iceland. In: Proceedings: 18th Workshop on Geothermal Reservoir Engineering, Stanford University, CA, USA, 1993.
Buscarlet E, Moon H, Wallis I, Quinao J. Reservoir tracer test at the Ngatamariki Geothermal Field. In: Proceedings: 37rd New Zealand Geothermal Workshop, Taupo, 2015.
Croucher A, O'Sullivan MJ. Approaches to local grid refinement in TOUGH2 models. In: Proceedings: 35th New Zealand Geothermal Workshop, Rotorua, New Zealand; 2013.

Croucher A. PyTOUGH: a Python scripting library for automating TOUGH2 simulations. In: Proceedings: 33rd New Zealand Geothermal Workshop, Auckland, New Zealand, 2011.
Čypaitė V, Ingimarsson H. Nesjavallavirkjun. Groundwater Temperature Measurements in 2017. Iceland GeoSurvey, Report No. ÍSOR-17160. 2017.
Čypaitė V. Effluent Flow from Nesjavellir Power Plant. Iceland GeoSurvey, Report No. ÍSOR-2018/039. 2018.
Diaz AR, Kaya E, Zarrouk SJ. Reinjection in geothermal fields - a worldwide review update. Renew Sustain Energy Rev. 2016;53:105–62.
Franzson H, Gunnlaugsson E, Árnason K, Sæmundsson K, Steingrímsson B, Harðarson BS. The Hengill Geothermal System, Conceptual Model and Thermal Evolution. In: Proceedings: World Geothermal Congress 2010, Bali, Indonesia, 2010.
Franzson H. Nesjavellir-Borholujarðfræði, vatnsgengd í jarðhitageymi. Orkustofnun, Report No. OS-88046/JHD-09. 1988.
Franzson H. Hydrothermal evolution of the Nesjavellir high-temperature system, Iceland. In Proceedings: World Geothermal Congress 2000, Kyushu-Tohoku, Japan, 2000.
Gíslason G. Nesjavellir co-generation plant, Iceland. Flow of geothermal steam and noncondensable gases. In: Proceedings: World Geothermal Congress 2000, Kyushu-Tohoku, Japan, 2000.
Gunnarsson G, Aradóttir ES. The Deep roots of geothermal systems in volcanic areas: boundary conditions and heat sources in reservoir modeling. Transp Porous Media. 2014;1081:43–59. https://doi.org/10.1007/s11242-014-0328-1.
Gunnarsson G, Arnaldsson A, Oddsdóttir AL. Model Simulations of the Hengill Area, Southwestern Iceland. Transp Porous Media. 2011;90:3–22. https://doi.org/10.1007/s11242-010-9629-1.
Gunnarsson G, Tómasdóttir S, Klüpfel S, Westergren Á, Björnsson GB. Managing the Production Fields in the Hengill Area. In Proceedings: World Geothermal Congress 2020, Reykjavik, Iceland, 2020.
Hafstað ÞH, Níelsson S. Nesjavallavirkjun. Hitamælingar á affallssvæðinu í október 2013. Iceland GeoSurvey, Report No. ÍSOR-13087. 2013.
Hafstað ÞH, Vilmundardóttir EG, Kristjánsson BR, Nesjavellir. Rannsóknarborholur í hraunununm á affallssvæði virkjunarinnar. Iceland GeoSurvey, ÍSOR-2007/058. 2007.
Hafstað ÞH, Nesjavellir. Mælingar í eftirlitsholum í Nesjahrauni. Orkustofnun, Report No. ÞHH-2000a-06. 2000a.
Hafstað ÞH, Nesjavellir. Um eftirlitsholu norðan við orkuverið. Orkustofnun, Report No. ÞHH-2000b-18. 2000b.
Hafstað ÞH, Nesjavellir. Boranir á afrennslissvæði. Staðan um aldamót. Orkustofnun, Report No. ÞHH-2000c-22. 2000c.
Hafstað ÞH, Nesjavellir. Hitamælingar á afrennslissvæði. Orkustofnun, Report No. ÞHH-2001a-13. 2001a.
Hafstað ÞH, Nesjavellir. Um affallið í hrauninu. Orkustofnun, Report No. ÞHH-2001b-19. 2001b.
Hafstað ÞH. Niðurrennslisholurnar NN-3 og NN-4 á Nesjavöllum. Iceland GeoSurvey, Report No. ÍSOR-ÞHH-2003/068. 2003.
Hafstað ÞH, Nesjavallavirkjun. Hitamælingar á affallssvæði í nóvember 2014. Iceland GeoSurvey, Report No. ÍSOR-14072. 2014.
Ingimarsson H, Hafstað ÞH, Nesjavallavirkjun. Hitamælingar á affallssvæði í nóvember 2015. Iceland GeoSurvey, Report No. ÍSOR-15064. 2015.
Ingimarsson H, Čypaitė V, Hafstað ÞH. Nesjavallavirkjun. Hitamælingar á affallssvæði í nóvember 2016. Iceland GeoSurvey, Report No.ÍSOR-16064. 2016.
Kamila Z, Kaya E, Zarrouk SJ. Reinjection in geothermal fields: an updated worldwide review 2020. Geothermics. 2021;89: 101970. https://doi.org/10.1016/j.geothermics.2020.101970.
Kaya E, O'Sullivan MJ, Brockbank K. Reinjection into liquid-dominated two-phase geothermal systems. In: Proceedings: 36th Workshop on Geothermal Reservoir Engineering, Stanford University, California, USA. 2011.
Kjaran SP, Egilson D. Nesjavellir. Áhrif affallsvatns frá fyrirhugaðri jarðvarmavirkjun á vatnsból við Grámel (86–03). Reykjavík. Internal Verkfræðistofan Vatnaskil report. 1986.
Kjaran SP, Egilson D. Ferlun grunnvatns á Nesjavöllum. Reykjavík. Internal Verkfræðistofan Vatnaskil report. 1987.
Kristinsson SG, Hafstað ÞH. Nesjavellir. Hitamælingar í eftirlitsholum á affallssvæði í nóvember 2010. Iceland GeoSurvey, Report No. ÍSOR-11033. 2011.
Kristinsson SG, Níelsson S. Nesjavellir. Hitamælingar í eftirlitsholum á affallssvæði í júní 2012. Iceland GeoSurvey, Report No. ÍSOR-12075. 2012.
Maliva RG. Aquifer characterization techniques: schlumberger methods in water resources evaluation. Hydrogeology. 2016. https://doi.org/10.1007/978-3-319-32137-0.
O'Sullivan J, O'Sullivan MJ, Croucher A. Improvements to the AUTOUGH2 Supercritical Simulator with Extension to the Air-Water Equation-of-State. GRC Trans. 2016;40:921–30.
Pham M, Klein C, Ponte C, Cabeças R, Martins R, Rangel G.. Production/Injection optimization using numerical modeling at Ribeira Grande, São o Miguel, Azores, Portugal. In: Proceedings of the World Geothermal Congress 2010, Bali. 2010.
Pruess K, Oldenburg CM, Moridis GJ. TOUGH2 User's Guide Version 2. Earth Sciences Division, Lawrence Berkeley National Laboratory. Berkeley CA, USA . LBNL-43134. 1999.
Pruess K, Narasimhan NT. A practical method for modeling fluid and heat flow in fractured porous media. Soc Petrol Eng J. 1985;251:14–26. https://doi.org/10.2118/10509-PA.
Ratouis TMP, Snæbjörnsdóttir SÓ, Voigt MJ, Sigfússon B, Gunnarsson G, Aradóttir ES, Hjörleifsdóttir V. Carbfix 2: A transport model of long-term CO2 and H2S injection into basaltic rocks at Hellisheidi. SW-Iceland, Int J Greenhouse Gas Control. 2022;114: 103586. https://doi.org/10.1016/j.ijggc.2022.103586.
Ratouis TMP, Snæbjörnsdóttir SO, Gunnarsson G, Gunnarsson I, Kristjánsson BR, Aradóttir ES. Modelling the Complex Structural Features Controlling Fluid Flow at the CarbFix2 Reinjection Site, Hellisheiði Geothermal Power Plant, SW-Iceland. In: Proceeding: 44th Workshop on Geothermal Reservoir Engineering, Stanford University, CA, USA, 2019.
Rose PE, Benoit WR, Kilbourn PM. The application of the polyaromatic sulfonates as tracers in geothermal reservoirs. Geothermics. 2001;30(6):617–40.
Shook MJ, Forsmann HJ. Tracer Interpretation Using Temporal Moments on a Spreadsheet, Idaho National Laboratory, Report No. INL/EXT-05-00400. 2005. https://inldigitallibrary.inl.gov/sites/sti/sti/3028333.pdf. Accessed 12 October 2021.

Shook MG. A systematic method for tracer test analysis: an example using beowawe tracer data. In: Proceedings, 30th Workshop on Geothermal Reservoir Engineering, Stanford University, CA, USA, 2005.
Snæbjörnsdóttir S, Wiese F, Fridriksson T, Ármansson H, Einarsson GM, Gislason SR. CO2 storage potential of basaltic rocks in Iceland and the oceanic Ridges. Energy Procedia. 2014;63:4585–600. https://doi.org/10.1016/j.egypro.2014.11.491.
Snorrason SS, Malmquist HJ, Ingólfsdóttir HB, Ingimundardóttir Þ, Ólafsson JS. Effects of geothermal effluents on microbenthic communities in a pristine sub-Arctic lake. Inland Waters. 2011;13:146–57. https://doi.org/10.5268/IW-1.3.363.
Stefánsson V. Geothermal reinjection experience. Geothermics. 1997;26:99–139. https://doi.org/10.1016/S0375-6505(96)00035-1.
Steingrímsson B, Bodvarsson GS, Gunnlaugsson E, Gíslason G, Sigurdsson Ó. Modelling studies of the Nesjavellir geothermal field, Iceland. In: Proceedings: World Geothermal Congress 2000, Kyushu-Tohoku, Japan, 2000.
Stevenson JA, Mitchell NC, Mochrie F, Cassidy M, Pinkerton H. Lava penetrating water: the different behaviours of pahoehoe and 'a'a at the Nesjahraun, Þingvellir. Iceland Bull Volcanol. 2012;74:33–46. https://doi.org/10.1007/s00445-011-0480-1.
Þorbjörnsson D, Ólafsson GE, Hafstað ÞH Nesjavellir. Hitamælingar í eftirlitsholum á affallssvæði í maí 2009. Iceland GeoSurvey, Report No. ÍSOR-09052. 2009.
Wagner W, Pruß A. The IAPWS formulation 1995 for the thermodynamic properties of ordinary water substance for general and scientific use. J Phys Chem. 2002;312:387–535. https://doi.org/10.1063/1.1461829.
Yeh A, Croucher A, O'Sullivan MJ. Recent developments in the AUTOUGH2 simulator. In: Proceedings: TOUGH Symposium, Berkeley, California, 2012.
Yeh A, Croucher AE, O'Sullivan MJ. TIM–Yet another Graphical Tool For TOUGH2. In: Proceeding: 35th New Zealand Geothermal Workshop, Rotorua, New Zealand, 2013.
Zakharova OK, Spichak VV. Geothermal fields of Hengill Volcano, Iceland. J Volcanol Seismol. 2012;6:1–14. https://doi.org/10.1134/S074204631201006X.
Zarandi SSMM, Ivarsson G. A Review on Waste Water Disposal At the Nesjavellir Geothermal Power Plant. In: Proceedings: World Geothermal Congress 2010, Bali, Indonesia, 2010.

Publisher's Note